tvst

Retina

Radial and Tangential Retinal Magnifications as Functions of Visual Field Angle Across Spherical, Oblate, and Prolate Retinal Profiles

Gareth D. Hastings[1], Martin S. Banks[1], and Austin Roorda[1]

[1] Herbert Wertheim School of Optometry and Vision Science, University of California Berkeley, Berkeley, CA, USA

Correspondence: Gareth D. Hastings, Herbert Wertheim School of Optometry and Vision Science, University of California Berkeley, 485 Minor Hall, Berkeley, CA 94720, USA. e-mail: gdhastings1@gmail.com, gdhastings@berkeley.edu

Received: May 11, 2022
Accepted: August 11, 2022
Published: September 19, 2022

Keywords: retinal magnification factor; distortion; prolate; oblate; nodal point

Citation: Hastings GD, Banks MS, Roorda A. Radial and tangential retinal magnifications as functions of visual field angle across spherical, oblate, and prolate retinal profiles. Transl Vis Sci Technol. 2022;11(9):10, https://doi.org/10.1167/tvst.11.9.10

Purpose: To provide a tool for calculating radial and tangential retinal magnifications as functions of field angle and retinal shape and to articulate patterns of magnification across the retina for monocular and binocular combinations of prolate-, oblate-, and spherical-shaped retinas.

Methods: Formulae were derived to calculate radial and tangential retinal magnifications (mm/deg) from field angle (degrees), retinal asphericity (unitless conic constant), retinal vertex radius of curvature (mm), and nodal point position (mm). Monocular retinal magnifications were determined for eyes with prolate, spherical, and oblate retinas as functions of field angle. Bilateral differences in magnifications were examined for combinations of those eyes.

Results: Retinal shape substantially affects magnification profiles even for eyes with the same axial length. Greatest magnification changes across a retina and between eyes, as well as greatest increase in radial–tangential differences (distortion), occur with prolate retinas. Binocular magnification differences were smallest for oblate retinas. Nodal points anterior to the vertex center of curvature and oblate asphericity both cause field-dependent reductions in magnification relative to the fovea (barrel distortion), whereas nodal points posterior to vertex center of curvature and prolate asphericity cause the opposite (pincushion distortion). Retinal magnification differences due to eye shape are much greater than aniseikonia thresholds and chromatic differences in magnification. A spreadsheet tool implements the magnification calculations.

Conclusions: Local retinal magnifications as functions of field angle have substantial effects on objective applications (imaging retinal anatomy) and subjective experiences (aniseikonia) and quantify an ocular property that differs across eye shapes and refractive errors.

Translational Relevance: Methods are provided to customize the calculation of radial and tangential magnifications across the retina for individual eyes, which will bolster the multifactorial study of the effects of foveal and peripheral optics across eye shapes and refractive errors.

Introduction

Magnification is a fundamental attribute of ocular optics that can relate distance units, such as millimeters, to visual angle units, typically degrees, on the retina. Because the retinal image is two dimensional, magnification at any point is commonly considered in two components (along two meridians). As will be demonstrated, *radial* magnification relates to the local shape of the retina in a plane (such as a magnetic resonance imaging [MRI] section of an eye[1,2]), and *tangential* magnification relates to the distance that a hypothetical ray of light travels to the retina. In a one-dimensional ray diagram, the classical object–image relationship is only illustrated in the radial dimension (Fig. 1B); the tangential dimension is perpendicular to the radial plane (Fig. 1A). Changes in magnification over the

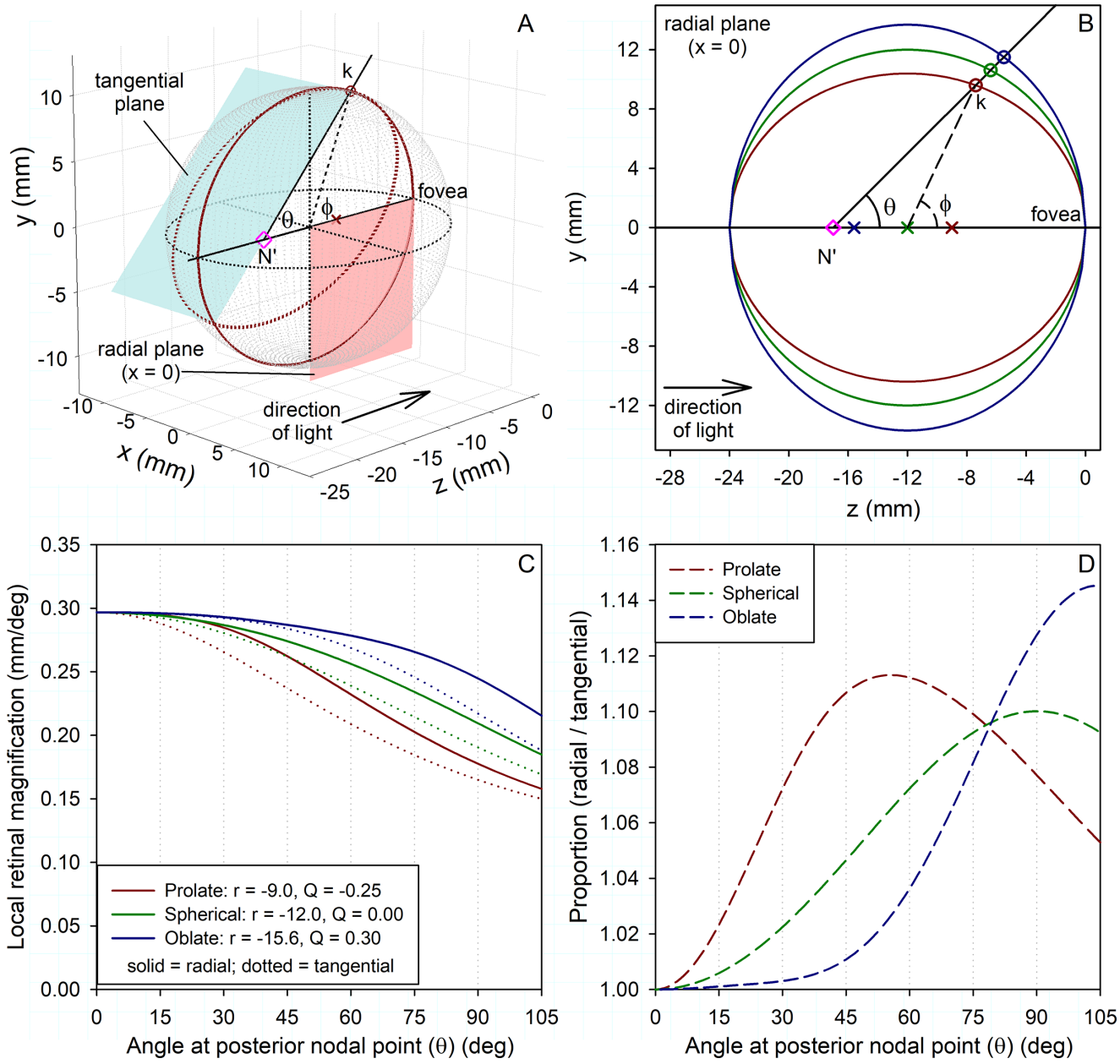

Figure 1. On-axis (foveal) axial length cannot unambiguously inform retinal shape or magnification as a function of field angle. (A) Scheme for representing an eyeball (*translucent gray*) as an ellipsoid of rotation around the *z*-axis. The fovea is located at the origin (0,0,0). A ray (*solid black line*) emerges from the posterior nodal point (*N'*; *pink diamond*), 17 mm from the fovea (7 mm from the cornea), and intersects the retina at *k*. Radial magnification is defined along the *red solid ellipse* (in the plane $x = 0$; partially plotted in *pale red*). Tangential magnification is defined along the *dotted red ellipse*, which is orthogonal to the radial ellipse at point *k* and is in the *cyan* (tangential) plane (illustrated for $x < 0$). The *dashed black line* connects point *k* to the geometric center of the ellipsoid. Supplementary Materials include an animation of (A). (B) Radial profiles representing three anatomically plausible[1,27] eyes with theoretical axial lengths of 24 mm (*red* is a prolate ellipse, *green* is a circle, *blue* is an oblate ellipse). Definitions of these profiles in terms of vertex radii of curvature *r* (indicated by × symbols) and conic constants *Q* (see legend for panel C) are described in the Methods. (C) Due to different retinal shapes, both radial and tangential retinal magnifications (*solid* and *dotted lines*, respectively) differ substantially across the three eyes as functions of field angle. (D) Proportions (aspect ratio) of radial magnification/tangential magnification as function of field angle. There is asymmetry between the radial and tangential dimensions for all eye shapes; as a function of field angle, this increases much more rapidly for the prolate profile (retinal images are also illustrated in Fig. 6).

visual field and differences between radial and tangential magnifications are what is classically referred to as *distortion*.

These local retinal magnifications are relevant to clinical applications of objectively resolving anatomical structures using adaptive optics[3,4] or optical

coherence tomography,[5,6] when computing light irradiance across the retina,[7] and during focus-dependent surgical techniques such as photocoagulation.[8] Ocular magnification also affects subjective visual experience and is considered when minimizing aniseikonia during the prescription of spectacles[9,10] or intraocular lens powers,[11] as well as during low vision care of eyes with central vision loss[12] and in understanding the optical and visual quality of emmetropic versus myopic eyes.[13]

The adjusted axial length method proposed by Bennett et al.[14] is widely used to determine a foveal retinal magnification factor, but this method assumes that the retina and posterior focal planes of the eye coincide, which is the case in neither foveal ametropias nor in peripheral refractive errors. We show in this paper why magnification in and around the fovea is insensitive to retinal shape, and we focus on the more challenging case of calculating retinal magnification factors beyond the fovea.

How magnification changes as a function of visual field angle (away from the fovea) is of interest given that peripheral optics are important for signaling accommodative responses,[15] driving,[16] and mobility,[17] as well as in clinical perimetry.[18] Further, due to associations between off-axis optics and the onset and progression of myopia,[19] peripheral image quality is being increasingly considered in the design of free-form spectacle lenses,[20,21] custom and orthokeratology contact lenses,[22] and head-mounted displays.[23]

An essential consideration when studying magnification as a function of field angle is retinal shape, especially given potential associations between retinal shape and refractive errors[24] and how velocities of retinal images change across different retinal shapes during eye movements.[25] Popular methods[14,26] of projecting object space across the retina assume that the retina is spherical. The shortcoming of this assumption is illustrated in Figure 1B, where circular and elliptical profiles are plotted that represent three anatomically plausible retinal shapes.[1,27] These three eyes have the same theoretical on-axis axial lengths (24 mm), but, due to their different retinal shapes, magnification as a function of field angle differs substantially across the three retinas (Fig. 1C).

Popular methods of calculating magnification, such as that of Drasdo and Fowler,[26] are not readily customizable for the calculation of magnification in individual eyes. One goal of the present paper was to provide a tool for these calculations that could be implemented in spreadsheet software (see Supplementary Material). Given increased accessibility of technologies that quantify retina shape,[1,2,27–29] this tool allows magnification to be calculated over the retina for individual eye shapes analogous to the common presentation of relative peripheral refraction.[24]

The tool calculates retinal magnification as a function of (1) field angle, (2) nodal point position relative to the retina, and (3) retinal shape, where retinal shape is defined[1,27] as a circle, prolate ellipse, or oblate ellipse by a radius of curvature r and an aspheric conic constant Q. To demonstrate the calculations, we articulate monocular magnification patterns resulting from the interaction of the three variables and emphasize the effect of retinal shape. Changes in magnification across the retinas are also discussed in the context of classical concepts such as barrel and pincushion distortions, as well as applications such as ocular imaging, aniseikonia, chromatic differences in magnification, and binocular vision. Across these applications, we ask which errors would result (1) if peripheral magnification was assumed to equal magnification at the fovea, and (2) if the retina was assumed to be spherical when it is aspheric? A detailed derivation of the calculations and instructive methods for monitoring anatomical plausibility when performing the calculations are included in the Appendix.

Methods

We sought calculations of retinal magnification that could be performed in spreadsheet software. Although integrals and derivatives are employed in deriving the magnification equations, the resulting functions ultimately require only algebra and trigonometry. Here, methods are summarized; a full derivation of calculations and logic is provided in the Appendix. The methods are automated in a Microsoft Excel spreadsheet in the Supplementary Material.

Definitions, Conventions, and Assumptions

Retinal magnification is studied using an ocular nodal point convention. Although nodal points are strictly a paraxial concept, they are broadly employed in wide-angle applications [5,6,30,31] and have been shown to be in good agreement with real ray tracing over large field angles.[32] Using a nodal point convention simplifies the optical contributions of the refracting surfaces and media of an eye into a pair of locations. The classical concept is that a ray that travels at a particular angle toward the first (anterior) nodal point emerges from the optical system in the same direction, along a line that includes the second (posterior) nodal point. The conceptual path through both nodal points and the

fovea is known as the visual axis,[33,34] and field angle is described as the angle formed between a ray and the visual axis (θ in Fig. 1). We use the term *fixation* to refer to the object location conjugate to the retinal fovea, and *nodal point* (N') to refer to the posterior nodal point.

We consider the fovea as the origin (0,0,0) of a coordinate space with dimensions in millimeters (Figs. 1A, 1B). Field angles (θ) are plotted in degrees (calculations use radians); when an object is at fixation, the angle is 0°. Magnification is modeled up to a field angle of 105°, which covers the maximum extent of a healthy monocular visual field.[35] In this coordinate space, a two-dimensional section of retina can be described[1,27] using the conic section equation[36]

$$0 = y^2 - 2rz + (Q+1)z^2 \quad (1)$$

where y and z are Cartesian coordinates (Figs. 1A, 1B), r is the vertex radius of curvature (at the fovea), and Q is the conic constant that defines oblate ($Q > 0$; blue in Fig. 1B), spherical ($Q = 0$; green), prolate ($0 > Q > -1$; red), parabolic ($Q = -1$), and hyperbolic ($Q < -1$) profiles. Note that defining retinal shape with an elliptical conic section in Equation 1 is the general case, within which circular or spherical retinas are included.

Checking Anatomical Plausibility and Nodal Point Position

There are various methods of measuring retinal shape,[1,2,27–29] each of which visualizes a different angular extent of retina. The representation used in Figure 1B is similar to MRI studies[1,2] where a section of the entire eye globe is described by a single ellipse; this approach ensures that the fit ellipse is anatomically plausible. Virtues and limitations of different approaches are considered in the Discussion and Appendix.

However, if only a segment of retina has been fit and those fit parameters are extrapolated to define an entire eyeball, it is possible that an anatomically implausible ellipse could result, and the nodal point might be farther from the fovea than the hypothetical axial length (see Appendix). In such cases, we need to limit the calculation of magnification to the maximum y-value (immediately before the retina begins to curve back toward the visual axis). To check this plausibility, we begin by calculating axial length from the parameters that define the eye shape:

$$Axial\ length = \frac{-2r}{(Q+1)} \quad (2)$$

Recall that r is measured from the vertex to the center of curvature and is a negative distance. If the calculated axial length (Equation 2) is greater in magnitude than the distance from the nodal point (N') to the retina, then any ray will reach the retina irrespective of the angle at which it emerges from the nodal point, and magnification calculations do not have to be constrained. However, if the nodal point is farther from the retina than the hypothetical axial length, the maximum valid field angle where a ray from the posterior nodal point will intersect with the retinal asymptote is

$$\theta_m = \arctan\left(\frac{y_{geo}}{(z_{geo} - N')}\right) \quad (3)$$

where z_{geo} is half of the axial length from Equation 2 and y_{geo} is

$$y_{geo} = \sqrt{\frac{r^2}{(1+Q)}} \quad (4)$$

Calculation of Radial and Tangential Local Retinal Magnifications

As derived in the Appendix, radial magnification as function of field angle (θ) is calculated as the product of three values: (1) local relative magnification derived from the perimeter equation of an ellipse; (2) the size of the angle subtended at the geometric center (ϕ) by an angle subtending 1° at the nodal point (N'), which is calculated using classical geometry; and (3) the magnification relative to the geometric center at the ellipse vertex (fovea), calculated as

$$mag\,(0^\circ) = \frac{\pi\,|z_{geo}|}{180} \quad (5)$$

where $\pi/180$ is the conversion of 1° to radians.

Tangential magnification is calculated using Equation 5 and substituting the path length of the ray (from the nodal point to the retina) in the place of z_{geo}. The logic behind this calculation is also articulated in the Appendix.

Results

Using the methods summarized above, monocular radial and tangential retinal magnifications were calculated as a function of field angle for combinations of each category of retinal shape and nodal point position. These are reported in order of increasing complexity.

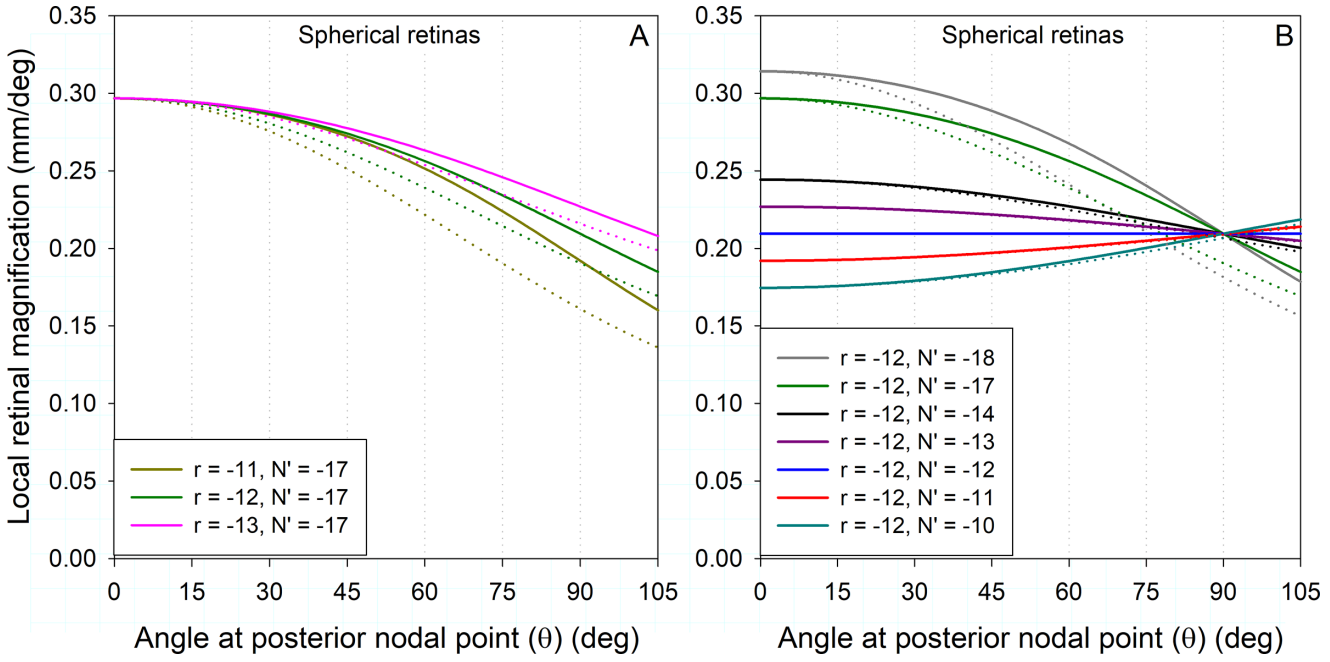

Figure 2. Local radial and tangential retinal magnifications (*solid* and *dotted lines*, respectively) as a function of field angle (θ) for different combinations of spherical retinal radii of curvature (r) and nodal point positions (N'). (A) Magnification at the fovea ($\theta = 0°$) is determined by the distance from N' to the retina irrespective of r. (B) As field angle increases, both magnifications decrease monotonically if N' is anterior to r (barrel distortion) and increase monotonically when N' is posterior (pincushion distortion). At the fovea, magnification is proportional to the distance from N' to the retina; it is constant (*blue trace*) when N' and (spherical) r are coincident, and all radial magnification curves converge to that constant value when $\theta = 90°$.

Spherical Retinas

Nodal Point at Spherical Retinal Center of Curvature

This simplest case is worth articulating because it is used in the classical geometric horopter.[33] When the retina is spherical and the nodal point is at the retinal center of curvature, local radial and tangential magnifications are constant as a function of field angle. Below, we show that these constant values depend on the radius of curvature of the spherical retina and not on the nodal point position. As the radius of curvature increases (flattens), the (constant) magnification increases. The ratio between (respectively constant) magnifications for different radii of curvature is the ratio between those radii of curvatures.

Because, here, the nodal point position and spherical retinal center of curvature coincide, the constant value of local magnification equals the length (in millimeters) of retinal arc subtended by 1° and can alternatively be calculated by the classical equation from circle geometry:

$$mag(\theta) = \frac{\pi |r|}{180} \quad (6)$$

which is equivalent to Equation 5. Thus, for spherical retinas with radii of curvature of 11, 12, and 13 mm and respective nodal points at their centers of curvatures, local radial and tangential magnifications are constant as functions of field angle at 0.192, 0.209, and 0.227 mm/deg, respectively. The example for 12 mm is included in Figure 2B.

Nodal Point Anterior or Posterior to Spherical Retinal Center of Curvature

In most eye models that assume a spherical retina, the nodal point is located anterior to the retinal center of curvature. For consistency with the aspheric retina examples that follow (where center of curvature refers to vertex radius of curvature), we include cases in which the nodal point is posterior to the retinal center of curvature.

When the nodal point is not coincident with the center of curvature of a spherical retina, local magnifications are no longer constant across field angles. At the fovea ($\theta = 0°$), radial and tangential magnifications are equal and determined by the nodal point position irrespective of retinal radius of curvature (Fig. 2A). This value can be calculated using Equation 6 and substituting r with the distance from N' to the retina. As field angle increases, both radial and tangential magnifications change monotonically: decreasing with eccentricity if the nodal point is anterior to the retinal

center of curvature (barrel distortion) and increasing with eccentricity when the nodal point is posterior (pincushion distortion). Tangential magnification is always less than radial magnification. At an angle of 90°, local radial magnification equals the constant value determined by the spherical retinal radius of curvature (see above) irrespective of the nodal point position. This is a consequence of circle geometry; a more general solution is provided for any retinal shape below.

The greater the difference between the nodal point position and the spherical retinal center of curvature, the greater the changes in both magnifications with field angle, which range from zero, when the points coincided, to up to 43% and 50% changes in radial and tangential magnifications, respectively, for the conditions modeled here (Fig. 2). Eyes that are mathematically *similar* (scaled versions of each other) have the same relative patterns of radial and tangential magnifications as a function of field angle.

Aspheric Retinas

In the preceding section with spherical retinas, modeled axial length could be estimated as $2r$; however, for aspheric retinas it is not that simple, and Equation 2 should be used. From Equation 2 one also notes the inverse linear relationship between the conic constant Q and axial length. Recall that the notion of radius of curvature is not as intuitive with aspheric shapes as for spherical retinas, and here it refers to the vertex radius of curvature (that is, at the fovea).

Nodal Point at the Aspheric Retinal Vertex Center of Curvature

This case isolates the effects of retinal asphericity on magnification. At the fovea ($\theta = 0°$), radial and tangential magnifications are equal and are determined by the distance from the nodal point to the retina irrespective of the retinal vertex radius of curvature and/or asphericity. For any (coincident) aspheric vertex center of curvature and nodal point, prolate asphericity ($0 > Q > -1$) causes an increase in local magnification with increasing field angle (pincushion distortion), and oblate asphericity ($Q > 0$) causes a decrease in local magnification (barrel distortion) (Fig. 3). Tangential magnification is less than radial magnification. If the underlying vertex radius of curvature is changed, all magnification curves shift by a proportional amount.

Nodal Point Anterior or Posterior to Aspheric Retinal Vertex Center of Curvature

Again, at the fovea ($\theta = 0°$), radial and tangential magnifications are equal and determined by the distance from the nodal point to the retina irrespective of the retinal vertex radius of curvature and/or asphericity. As field angle increases (Fig. 4), both the nodal point position and asphericity affect the change in magnification. Nodal point positions anterior to the vertex center of curvature and oblate asphericity both cause a relative reduction in magnification with increasing field angle (barrel distortion), whereas nodal points posterior to the vertex center of curvature and prolate asphericity cause the opposite. Radial magnification curves (Fig. 4) converge to values (at $\theta = 90°$) determined by retinal shape (r and Q) irrespective of nodal point position. The dashed horizontal lines (constant magnification) through these convergence points in Figure 4 are empirically determined as the radial magnification values of equivalent spherical retinas with radii of curvature

$$r_{es} = \frac{2r}{(Q+2)} \tag{7}$$

where r and Q relate to the aspheric retina and r and r_{es} are negative distances. These equivalent spherical retinas intersect the aspheric retinas (in our coordinate space) at the point on the aspheric retinas where $z = y$. The magnifications for each r_{es} (dashed lines in Fig. 4) are calculated by substituting r_{es} for r in Equation 6.

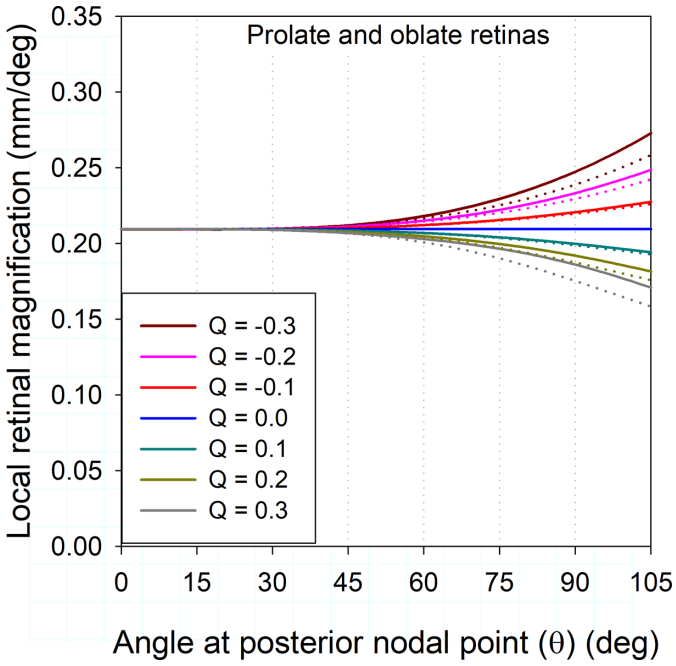

Figure 3. Isolated effect of retinal asphericity on radial and tangential magnifications (*solid* and *dashed lines*, respectively) as a function of field angle (θ). Across all traces, the retinal vertex center of curvature (r) and nodal point (N') are coincident at –12 mm. Note that, for the same magnitude of Q, prolate asphericities ($0 > Q > -1$) have a greater change in magnification than oblate asphericities ($Q > 0$).

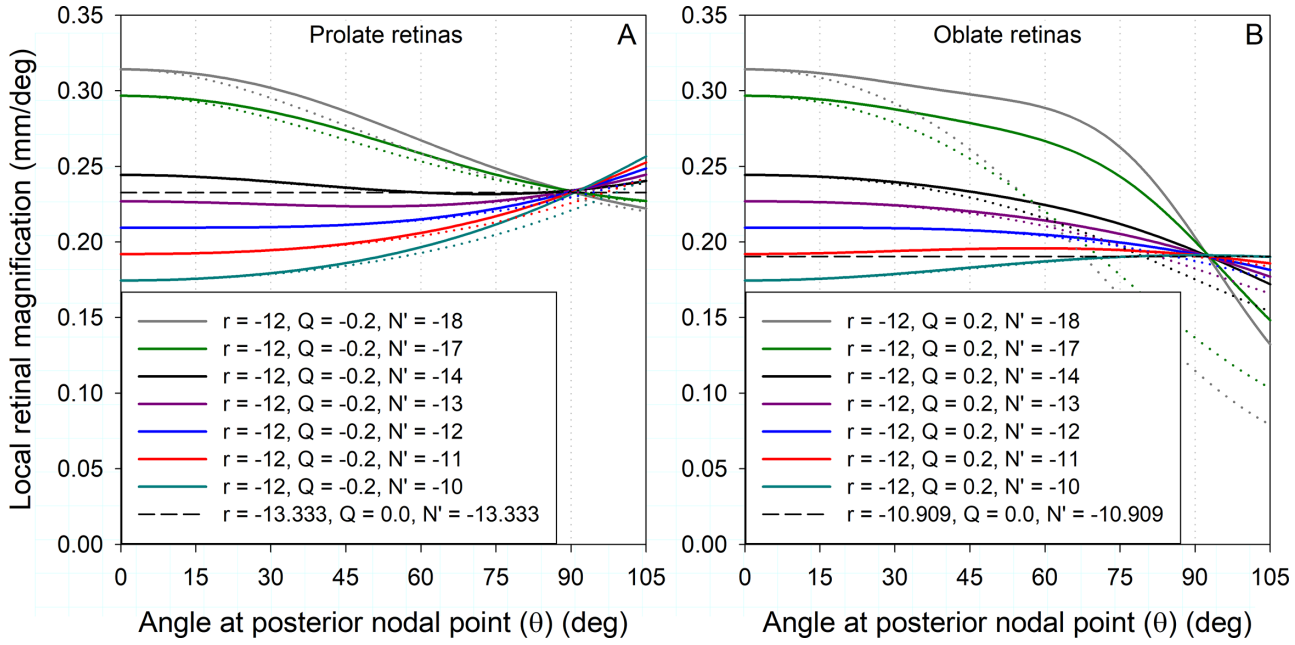

Figure 4. Local radial and tangential retinal magnifications (solid and dashed lines, respectively) as functions of field angle (θ) and the distance from the nodal point (N') to the retina for (A) prolate and (B) oblate asphericities. Across both panels, radial and tangential magnifications are equal at the fovea ($\theta = 0°$) and determined by the position of N' regardless of vertex radius of curvature (r) and/or asphericity (Q). Change in magnification with field angle depends on both Q and the position of N' relative to r. Magnification values to which all radial curves in each panel converge at $\theta = 90°$ are determined by r and Q and calculated using Equations 6 and 7.

The magnifications modeled in Figure 4 can be related to well-known clinical findings. If the prolate retina in Figure 4A was myopic[24] and corrected using spectacles, the nodal point position would be relatively nearer to the retina (lesser magnitudes of N' in the legend) than if that eye was corrected with contact lenses (or uncorrected) where the nodal point would be relatively nearer to the cornea.[37] The magnification curves echo the well-known minification caused by negative-power spectacles compared with contact lenses.

Although Figure 4 shows the effects of different nodal point positions when vertex radius of curvature and asphericity are held constant, it is also useful to refer to Figure 1 for examples where axial length and nodal point position are held constant. Figure 1C complements the patterns of magnification shown in Figure 4: Magnifications at fixation ($\theta = 0°$) are the same for the three curves because the nodal point positions are the same, and the decrease in local magnification with increasing field angle (barrel distortion) is influenced by the combination of radius of curvature and asphericity. Figure 1D shows the proportions of radial magnification/tangential magnification (aspect ratio) as a function of field angle. There is asymmetry between the radial and tangential dimensions in all eye shapes, which increases more rapidly for the prolate profile as a function of field angle away from the fovea.

Binocular Application

Figures 1 to 4 illustrate how retinal shape can affect monocular magnifications as a function of field angle. Subjectively, differences in magnification and retinal image size (aniseikonia) experienced between the two eyes when viewing binocularly also depend on retinal shape. Figure 5 shows how the present methods can be used to model aniseikonia as a function of field angle and object space for various combinations of retinal shapes. In these simulations, the interpupillary distance[38] is 63 mm. Symmetric convergence is modeled at 114 cm from the eyes, which was the median fixation distance for a collection of tasks[39]; changing this parameter has a small effect compared to that of eye shape.

Figures 5A and 5B illustrate the field angles subtended at each eye (θ_L and θ_R) by all points (e.g., point x) in a transverse plane in visual space spanning 400 × 400 mm. For each point in the plane, Figure 5C plots the unsigned difference in field angle (horizontal disparity) subtended at the two eyes ($|\theta_L - \theta_R|$). The angular data in Figures 5A, 5B, and 5C apply to all eye shapes. Figures 5D and 5E plot local radial retinal magnification corresponding to the subtended field angles (Figs. 5A, 5B) for left and right prolate retinas like the one in Figure 1. For each point in the plane, Figure 5F plots the difference in magnification

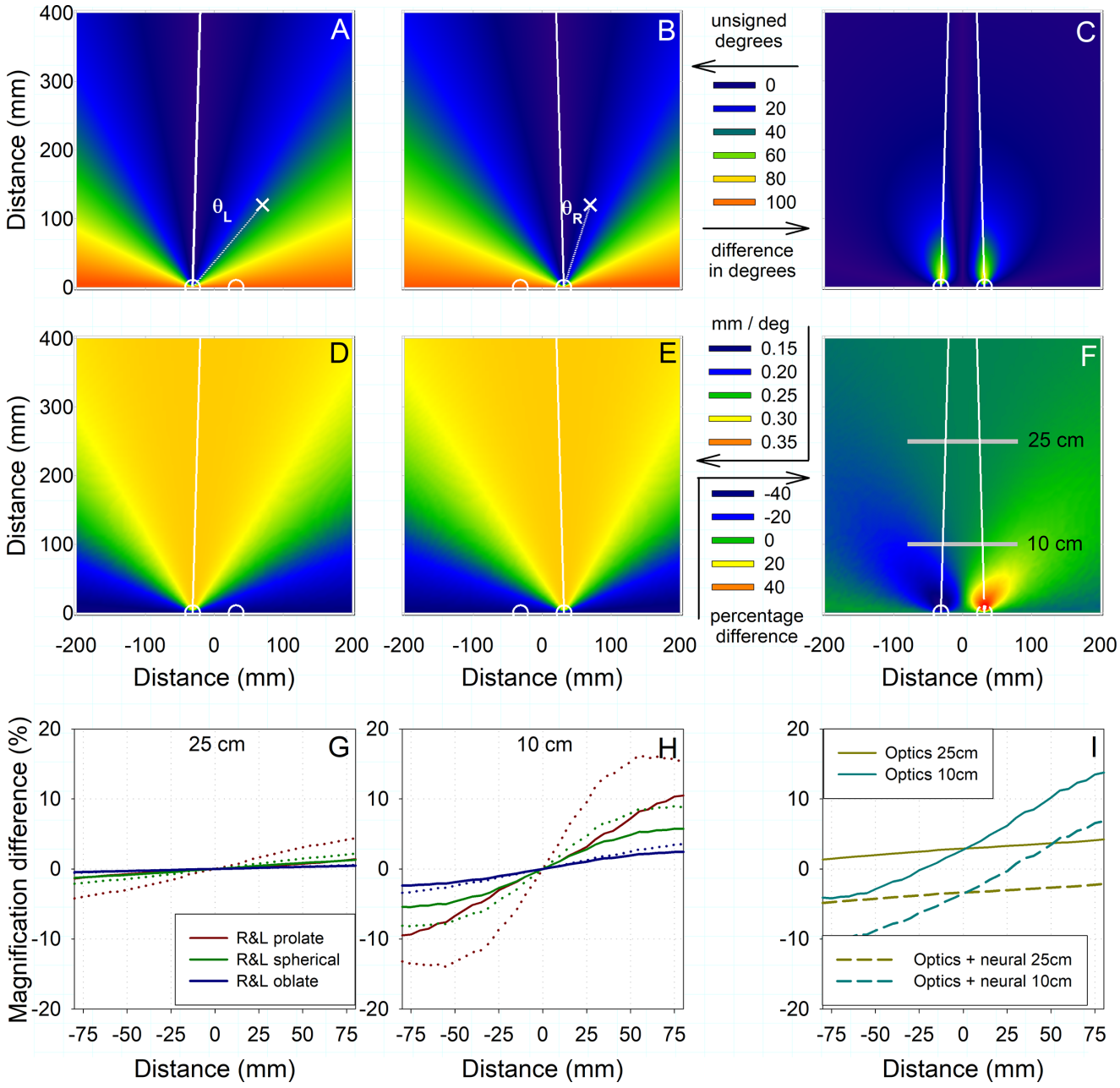

Figure 5. Differences in field angles and local retinal magnifications during binocular viewing. (A, B) Field angles subtended at the visual axis of left (θ_L) and right (θ_R) eyes by points in a transverse plane of visual space spanning 400 × 400 mm when the eyes are symmetrically converged (solid white lines) to 114 cm.[39] A representative point in the space is labeled X. (C) Unsigned differences (horizontal disparity) in angles formed at each eye across the plane ($|\theta_L - \theta_R|$). (A), (B), and (C) are common to all eye shapes. (D, E) Radial retinal magnification across the plane of visual space calculated from the angles in (A) and (B) for identical left and right prolate retinas (from Fig. 1; $r = -9$, $Q = -0.25$). (F) Percentage difference in magnification between right and left prolate retinas for each point in the plane [(right – left)/left * 100]. *Gray bars* indicate locations of data extracted at 25 cm and 10 cm from the eyes. (G, H) *Solid lines* are sections through surface plots of radial magnification like that in (F) for eyes of the same axial length (from Fig. 1) when right and left eyes have the same shape; *dotted lines* are for tangential magnification differences. (I) Plots where right and left eyes differ in shape (both prolate by different amounts) and axial lengths differ by 0.5 mm. Consequently, magnification also differs along the median plane of the head ($x = 0$). *Dashed curves* are after magnifications and are modified for neural aniseikonia (relative proportions of globe perimeters); this has only a small effect on the magnification difference between the eyes because the majority is optical in origin.

between the eyes as a percentage of the left eye values: Positive values indicate magnification relative to the left eye, and negative values indicate minification. Because Figures 5A to 5F model symmetric convergence of identical right and left eyes, there is no difference in magnification at the fixation point (not shown). The difference in magnification between right and left eyes increases the nearer that a point is to the eyes and illustrates, for example, the substantial differences in magnification that the optics of near-eye displays are engineered to overcome by placing the virtual image of the displays farther from the eyes than the actual displays. The application of these magnification methods to virtual reality head-mounted displays is a subset of the free-viewing case illustrated in Figure 5. The virtual image plane is typically at a distance roughly 65 cm to 2 m from the eyes, and accommodation posture—which impacts nodal point position—is expected to be relatively constant around that virtual image plane. Disparity rendering will drive convergence posture—which impacts the field angle relative to the nodal point. Although the optics of high-powered display lenses might distort virtual object space, geometric rendering calibrations should compensate for these distortions, and the three-dimensional space represented in Figure 5 becomes a plane at the virtual image distance from which light originates and projects across the retinas.

Figures 5G and 5H show one-dimensional sections through surfaces such as that plotted in Figure 5F. These illustrate the differences in magnification experienced between right and left eyes across the plane in visual space and are conceptually the converse of iso-magnification curves.[40,41] Whereas Figures 5D to 5F show radial magnification corresponding to the one condition where both eyes are prolate in shape, Figures 5G to 5I illustrate radial and tangential magnifications for many pairings of eye shapes at 25 cm and 10 cm from the eyes. Figures 5G and 5H treat right and left eyes as identical in shape (both prolate or both spherical or both oblate); Figure 5I models right and left eyes that are both prolate but by different amounts and consequently also have different axial lengths. Parameters of that left eye are like the prolate retinas in Figure 1 ($r = -9$; $Q = -0.25$; axial length = 24 mm) and parameters of the right eye are $r = -11.025$, $Q = -0.1$, and axial length = 24.5 mm. The nodal point of both eyes in Figure 5I was 7 mm from the cornea, mimicking vitreous chamber elongation that is common in anisometropia and aniseikonia.[9]

A neural component of aniseikonia was suggested when it was shown that equating the optical image sizes in both eyes (say, by following Knapp's law) did not resolve perceived aniseikonia in anisometropia.[9] Neural aniseikonia relates to the relative proportions of the retinas covered by the images, where, in a longer eye, an image of a given size covers a relatively smaller proportion of that retina than the same image size covers in a shorter eye. A simple account of this neural aniseikonia was incorporated into the dashed curves in Figure 5I by multiplying the radial magnification as a function of field angle in one eye by the ratio of the perimeters of the two globes (see Equation A15 and the below section, Extension of Data to Calculate Retinal Arc Length) and using the classical assumption of corresponding retinal points.[42] This has only a small effect on the difference in magnification experienced between the two eyes (Fig. 5I); the majority is caused by the differences in optical magnification described throughout this paper.

Discussion

Nodal Points

Although nodal points are theoretically a paraxial property of stigmatic systems, they have been generalized to astigmatic systems[34] and have been shown to be a good approximation of real ray tracing over wide field angles.[32] Despite that, at large field angles, the ray path through the entrance pupil (line of sight) can differ from the path modeled through the nodal points (visual axis),[43,44] we treat this difference as negligible, given that the main effects of the magnification results arise at angles larger than 5°. Although being a classic concept in optics, nodal points maintain modern applications such as in widefield[6] and ultra-widefield[5] optical coherence tomography, the design and troubleshooting of intraocular lens complications (such as farfield negative dysphotopsia[31]), determining posterior vitreous chamber dimensions,[30] modeling peripheral field loss,[45] and studying retinal structure–function relations dependent on field eccentricity.[18]

The baseline nodal point position of 7 mm from the cornea, which in most cases here is 17 mm from the retina (Figs. 1, 2, 5), is common in eye models[26,46] and instrumentation assumptions.[47] Multiple nodal point positions were modeled to illustrate the suitability of these methods for applications where the nodal point position changes, such as across different refractive errors[37] and during accommodation.[46] Nodal point positions also change when correcting ametropia with spectacle or trial lenses. Compensating hyperopia with a positive lens moves the nodal point anteriorly (toward the cornea), whereas compensating myopia with negative-powered spectacles moves the nodal points posteriorly (toward the retina).[48,49] Although changes to the nodal point position are minimally impacted by contact lens corrections[37] and

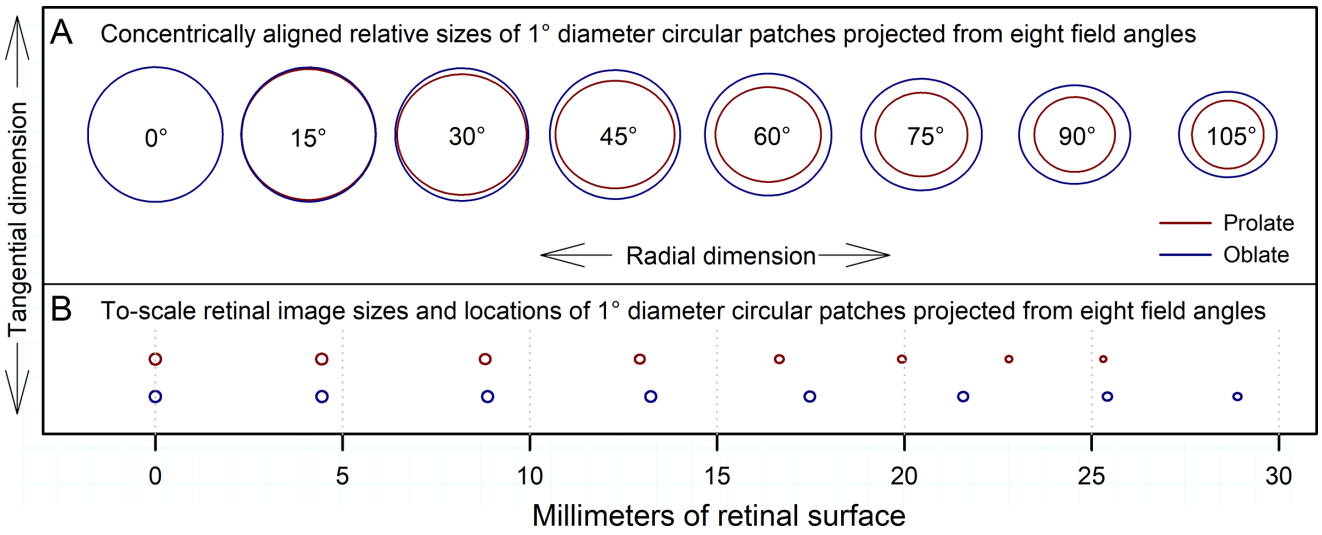

Figure 6. Effect of retina shape on radial and tangential magnifications and retinal image location. (A) Relative image proportions (aspect ratios) formed by a 1° diameter circular object on prolate and oblate retinas (from Fig. 1) across eight field angles, flattened into two dimensions. Only for 0° are the two images circular (radial and tangential are equal). (B) Location from the fovea (0 on the abscissa) where the retinal image is formed. Only for 0° do images form at the same distance (0 mm) from the fovea in both eyes. Note how visual space is minified across the prolate retina relative to the oblate retina.

can be completely avoided by using a Badal optometer, the compensation of ametropia with spectacle or trial lenses might complicate other imaging applications where assumptions have been made about nodal point positions. Nodal point positions for these magnification calculations either can be sensibly selected from the above-mentioned literature or can be estimated using customized or semi-customized biometric eye models in optical design software,[3,4] which can also include any corrective lenses.

Extent of Retina That Is Fit

An assumption that we employed was that one meridian of the entire retinal globe can be described by the fitting of a single ellipse. Although smaller angular segments[27] of retina could be more accurately fit, those methods can result in a larger range of values across individuals and implausible axial lengths if the fit parameters of the retinal segment are extrapolated to describe the entire globe. By beginning with a fit of the whole globe,[1,2] we are able to estimate and evaluate the anatomical plausibility of axial length and limit field angles to those that will reach the retina (Equations 2–4).

Radial and Tangential Magnifications

Both radial and tangential magnifications are cyclical as functions of the angle at the nodal point. Over the range of field angles (0°–105°) modeled here (Figs. 1–4), tangential magnification is less than radial and changes at a faster rate. Consequently, the difference plots (dotted lines) in Figures 5G to 5I are more pronounced for tangential than for radial magnification. Proportions of radial and tangential magnifications were shown for three eyes in Figure 1D. Figure 6A illustrates the relative effects of radial and tangential magnifications by superimposing images of a 1°-diameter circular object for prolate and oblate retinas from Figure 1 across eight field angles. In objective applications, such as retinal imaging, these differences affect the estimated sizes of retinal features and calculations of cell densities. This is the well-known motivation behind classical foveal estimates of retinal magnification factors.[14,26]

Extension of Data to Calculate Retinal Arc Length

Some classical models, when extended beyond the fovea, have treated the projected retinal image as flat[14] rather than projected across the curved retinal surface. In reality, different retinal shapes also result in different locations where a ray will intersect with (form an image on) the retina. The length along the retina from the fovea to the retinal image could be calculated using Equation A15 (perimeter of an ellipse) by modifying the integral (and coefficient factor) from $\pi/2$ to the desired field angle; it could be equivalently calculated (as was done for validation of this subanalysis) using

elliptic integrals.[50] Alternatively, that length along the retina from the fovea ($\theta = 0°$) to the retinal image for a ray emerging from the nodal point at $\theta = h°$ is the cumulative sum of magnifications (mm/deg) for angles from 0° to h° (essentially a discrete integral). Figure 6B plots retinal images of a 1°-diameter circle at the locations where they form on the retinas. One can appreciate how visual space is minified across the prolate retina relative to the oblate retina.

Practical Context of Magnification Differences

Monocular changes in magnification with field angle are discussed using the two questions from the Introduction: What magnification errors (differences) would result if (1) peripheral magnification was assumed to equal that of the fovea, and (2) if the retina was assumed to be spherical when it is aspheric? For each question, the magnification error at 30° and the maximum error in magnification at any field angle are considered.

First, across the eyes presented here with a 17-mm distance from nodal point to retina, assuming that peripheral magnification equals foveal magnification could result in radial and tangential errors (differences) at 30° of 4% and 11% (Fig. 1), respectively. Maximum errors (at larger angles) can approach 50% (Fig. 1) and 75% (Fig. 4B), respectively. Second, assuming that the retina is spherical when it is an anatomically plausible ellipse can result in radial and tangential magnification errors at 30° of 2% and 6% (Fig. 1), respectively. Maximum errors can surpass 20% (Fig. 3) and 60% (Fig. 4b), respectively.

These differences in magnification can be contexted in terms of transverse chromatic aberration (also known as chromatic difference in magnification), which is on the order of 1% difference between images at 400 and 700 nm.[51,52] Although differing spectral sensitivities play a role, the percentage of chromatic magnification differences with which the visual system is equipped to deal is substantially smaller than the effects demonstrated here from different retinal profiles.

Bilateral differences in magnification can cause diplopia and perceptual illusions, such as slant or curvature of a flat surface. Aniseikonia literature can help inform the question of what is a clinically significant subjective difference in binocular magnifications. These thresholds differ across visual orientations and are generally taken to refer to the most sensitive (that is, the vertical) meridian.[53]

The methods and data presented throughout most of this manuscript relate to the optical component of aniseikonia. This is comparable with data collected on instruments such as the space eikonometer,[54] which allows modification of monocular optical magnification to balance aniseikonia. Foveal data are plentiful and generally in agreement that typical levels of aniseikonia are less than a 2% difference in image size between the eyes and that a substantial impairment of binocular vision occurs at approximately 3% to 5% difference.[10,55]

It is expected that aniseikonia thresholds will change as a function of field angle away from the foveas; however, literature on the topic is not definitive. Ames and Ogle[56] summarized three studies and concluded that Panum's area (of single vision) grows relatively smaller with peripheral eccentricity. Crone and Leuridan[53] measured diplopia thresholds in degrees (asking whether two line targets appeared merged as single or distinct as double) and found a gradual increase in those diplopia thresholds as field angle increased beyond 10°. They believed that aniseikonia thresholds will also increase with field angle. Magnification differences between right and left eyes (Fig. 5) are substantially dependent on the distance of a point or plane from the eyes. For the examples presented, objects 25 cm from the eyes (Fig. 5G) resulted in magnification differences similar to the thresholds of Ames and Ogle[56] and Crone and Leuridan.[53] For objects nearer to the eyes (Figs. 5F and 5H) binocular magnification differences increased substantially and varied dependent on eye shape: In prolate retinas, these were considerably larger than the thresholds from the literature,[53,56] but oblate retinas shapes mitigated binocular magnification differences (Fig. 5).

Usage and Conclusions

The methods derived and demonstrated here are provided in a spreadsheet in the Supplementary Materials, where measured retinal shape[1,2,27–29] can be input or a selection of retinal shapes can be iteratively modeled, and local radial and tangential retinal magnifications as functions of field angle can be calculated. Again, nodal point position can be selected from the known assumptions of instrumentation,[47] literature,[37,46] generic eye models,[26,46] or custom eye models[3,4] and optical design software. The effects of retinal shape on local magnification across the retina are substantial and are important to consider in objective applications such as imaging retinal structures, subjective patient experiences such as aniseikonia and diplopia, and as an additional ocular property to bolster the multifactorial study of the effect of optics across eye shapes and refractive errors.

Acknowledgments

The authors thank Pavan Tiruveedhula for technical assistance. GDH was funded entirely by membership fees paid to the Center for Innovation in Vision and Optics by member companies.

Disclosure: **G.D. Hastings**, None; **M.S. Banks**, None; **A. Roorda**, None

References

1. Atchison D, Pritchard N, Schmid K, Scott D, Jones C, Pope J. Shape of the retinal surface in emmetropia and myopia. *Invest Ophthalmol Vis Sci*. 2005;46(8):2698–2707.
2. van Vught L, Dekker C, Stoel B, Luyten G, Beenakker J. Evaluation of intraocular lens position and retinal shape in negative dysphotopsia using high-resolution magnetic resonance imaging. *J Cataract Refract Surg*. 2021;47(8):1032–1038.
3. Li K, Tiruveedhula P, Roorda A. Intersubject variability of foveal cone photoreceptor density in relation to eye length. *Invest Ophthalmol Vis Sci*. 2010;51(12):6858.
4. Wang Y, Bensaid N, Tiruveedhula P, Ma J, Ravikumar S, Roorda A. Human foveal cone photoreceptor topography and its dependence on eye length. *eLife*. 2019;8(e47148):1–21.
5. Kolb J, Klein T, Kufner C, Wieser W, Neubauer A, Huber R. Ultra-widefield retinal MHz-OCT imaging with up to 100 degrees viewing angle. *Biomed Opt Express*. 2015;6(5):1534.
6. Mohler K, Draxinger W, Klein T, et al. Combined 60° wide-field choroidal thickness maps and high-definition en face vasculature visualization using swept-source megahertz OCT at 1050 nm. *Invest Ophthalmol Vis Sci*. 2015;56(11):6284.
7. Kooijman A, Witmer FK. Ganzfield light distribution on the retina of human and rabbit eyes: calculations and in vitro measurements. *J Opt Soc Am A*. 1986;3(12):2116.
8. Lotmar W. Theoretical eye model with aspherics. *J Opt Soc Am*. 1971;61(11):1522.
9. Bradley A, Rabin J, Freeman R. Nonoptical determinants of aniseikonia. *Invest Ophthalmol Vis Sci*. 1983;24(4):507–512.
10. Burian H. Clinical significance of anisekonia. *Arch Ophthalmol*. 1943;29(1):116–133.
11. Atchison D, Rozema J. Retinal image size in pseudophakia. *Ophthalmic Physiol Opt*. 2021;41(6):1222–1230.
12. Costela F, Woods R. The impact of field of view on understanding of a movie is reduced by magnifying around the center of interest. *Transl Vis Sci Technol*. 2020;9(8):6.
13. Coletta N, Watson T. Effect of myopia on visual acuity measured with laser interference fringes. *Vision Res*. 2006;46(5):636–651.
14. Bennett A, Rudnicka A, Edgar D. Improvements on Littmann's method of determining the size of retinal features by fundus photography. *Graefes Arch Clin Exp Ophthalmol*. 1994;232(6):361–367.
15. Labhishetty V, Cholewiak S, Banks M. Contributions of foveal and non-foveal retina to the human eye's focusing response. *J Vis*. 2019;19(12):18.
16. Wood J, Troutbeck R. Effect of restriction of the binocular visual field on driving performance. *Ophthalmic Physiol Opt*. 1992;12(3):291–298.
17. Patino C, McKean-Cowdin R, Azen S, Allison J, Choudhury F, Varma R. Central and peripheral visual impairment and the risk of falls and falls with injury. *Ophthalmology*. 2010;117(2):199–206.e1.
18. Antwi-Boasiako K, Carter-Dawson L, Harwerth R, Gondo M, Patel N. The relationship between macula retinal ganglion cell density and visual function in the nonhuman primate. *Invest Ophthalmol Vis Sci*. 2021;62(1):5.
19. Smith E, Hung L, Huang J. Relative peripheral hyperopic defocus alters central refractive development in infant monkeys. *Vision Res*. 2009;49(19):2386–2392.
20. Bowrey H, Zeng G, Tse D, et al. The effect of spectacle lenses containing peripheral defocus on refractive error and horizontal eye shape in the guinea pig. *Invest Ophthalmol Vis Sci*. 2017;58(5):2705–2717.
21. Sankaridurg P, Donovan L, Varnas S, et al. Spectacle lenses designed to reduce progression of myopia: 12-month results. *Optom Vis Sci*. 2010;87(9):631–641.
22. Kang P, Gifford P, Swarbrick H. Can manipulation of orthokeratology lens parameters modify peripheral refraction? *Optom Vis Sci*. 2013;90(11):1237–1248.
23. Yang J, Liu W, Lv W, et al. Method of achieving a wide field-of-view head-mounted display with small distortion. *Opt Lett*. 2013;38(12):2035–2037.
24. Wallman J, Winawer J. Homeostasis of eye growth and the question of myopia. *Neuron*. 2004;43(4):447–468.
25. Rucci M, Victor J. Perspective: can eye movements contribute to emmetropization? *J Vis*. 2018;18(7):10.

26. Drasdo N, Fowler C. Non-linear projection of the retinal image in a wide-angle schematic eye. *Br J Ophthalmol*. 1974;58(8):709–714.
27. Faria-Ribeiro M, López-Gil N, Navarro R, Lopes-Ferreira D, Jorge J, González-Méijome J. Computing retinal contour from optical biometry. *Optom Vis Sci*. 2014;91(4):430–436.
28. Verkicharla P, Suheimat M, Pope J, et al. Validation of a partial coherence interferometry method for estimating retinal shape. *Biomed Opt Express*. 2015;6(9):3235–3247.
29. Kuo A, Verkicharla P, McNabb R, et al. Posterior eye shape measurement with retinal OCT compared to MRI. *Invest Ophthalmol Vis Sci*. 2016;57(9):OCT196–OCT203.
30. Gilmartin B, Nagra M, Logan N. Shape of the posterior vitreous chamber in human emmetropia and myopia. *Invest Ophthalmol Vis Sci*. 2013;54(12):7240.
31. Ramasubramanian V, Meyer D, Kollbaum P, Bradley A. Experimental model of far temporal field negative dysphotopsia generated in phakic eyes. *Invest Ophthalmol Vis Sci*. 2020;61(5):24.
32. Simpson M. Scaling the retinal image of the wide-angle eye using the nodal point. *Photonics*. 2021;8(7):284.
33. Turski J. On binocular vision: the geometric horopter and cyclopean eye. *Vision Res*. 2016;119:73–81.
34. Harris W. Nodes and nodal points and lines in eyes and other optical systems: nodes and nodal points and lines. *Ophthalmic Physiol Opt*. 2009;30(1):24–42.
35. Spector RH. Visual fields. In: Walker HK, Hall WD, Hurst JW, eds. *Clinical Methods: The History, Physical, and Laboratory Examinations*. 3rd ed. Boston: Butterworths; 1990.
36. Smith W. *Modern Optical Engineering: The Design of Optical Systems*. 3rd ed. New York: McGraw-Hill; 2000.
37. Christaras D, Rozema J, Ginis H. Ocular axial length and straylight. *Ophthalmic Physiol Opt*. 2020;40(3):316–322.
38. Dodgson NA. Variation and extrema of human interpupillary distance. In: Bola MT, Woods AJ, Merritt JO, Benton SA, eds. *Stereoscopic Displays and Virtual Reality Systems XI*. Bellingham, WA: SPIE; 2004:36–46.
39. Sprague W, Cooper E, Tošić I, Banks M. Stereopsis is adaptive for the natural environment. *Sci Adv*. 2015;1(4):e1400254.
40. Ogle K. An analytical treatment of the longitudinal horopter; its measurement and application to related phenomena, especially to the relative size and shape of the ocular images. *J Opt Soc Am*. 1932;22(12):665–728.
41. Vlaskamp B, Filippini H, Banks M. Image-size differences worsen stereopsis independent of eye position. *J Vis*. 2009;9(2):17.1–17.13.
42. Hillis J, Banks M. Are corresponding points fixed? *Vision Res*. 2001;41(19):2457–2473.
43. Applegate R, Thibos L, Bradley A, et al. Reference axis selection: subcommittee report of the OSA Working Group to establish standards for measurement and reporting of optical aberrations of the eye. *J Refract Surg*. 2000;16(5):S656–S658.
44. Nowakowski M, Sheehan M, Neal D, Goncharov A. Investigation of the isoplanatic patch and wavefront aberration along the pupillary axis compared to the line of sight in the eye. *Biomed Opt Express*. 2012;3(2):240–258.
45. Apfelbaum H, Peli E. Tunnel vision prismatic field expansion: challenges and requirements. *Transl Vis Sci Technol*. 2015;4(6):8.
46. Blaker J. Toward an adaptive model of the human eye. *J Opt Soc Am*. 1980;70(2):220–223.
47. Turpin A, McKendrick A. Improving personalized structure to function mapping from optic nerve head to visual field. *Transl Vis Sci Technol*. 2021;10(1):19.
48. Pascal J. The cardinal points in corrected ametropia. *Br J Ophthalmol*. 1950;34(4):261–264.
49. Harris W. Pascal's ring, cardinal points, and refractive compensation. *Vision Res*. 2011;51(14):1679–1685.
50. Suheimat M, Zhu H, Lambert A, Atchison D. Relationship between retinal distance and object field angles for finite schematic eyes. *Ophthalmic Physiol Opt*. 2016;36(4):404–410.
51. Zhang X, Bradley A, Thibos L. Experimental determination of the chromatic difference of magnification of the human eye and the location of the anterior nodal point. *J Opt Soc Am A*. 1993;10(2):213–220.
52. Zhang X, Thibos L, Bradley A. Relation between the chromatic difference of refraction and the chromatic difference of magnification for the reduced eye. *Optom Vis Sci*. 1991;68(6):456–458.
53. Crone R, Leuridan O. Tolerance for aniseikonia: I. Diplopia thresholds in the vertical and horizontal meridians of the visual field. *Albrecht von Graefes Arch Klin Ophthalmol*. 1973;188(1):1–16.
54. Ames A. The Space Eikonometer test for aniseikonia. *Am J Ophthalmol*. 1945;28(3):248–262.
55. Achiron L, Witkin N, Primo S, Broocker G. Contemporary management of aniseikonia. *Surv Ophthalmol*. 1997;41(4):321–330.

56. Ames A, Ogle K. Size and shape of ocular images III. *Arch Ophthalmol*. 1932;7(6):904–924.
57. Chandrupatla T, Osler T. The perimeter of an ellipse. *Math Sci*. 2010;35(2):122–131.
58. Hastings G, Roorda A. Modeling optical and visual image quality across the retina. *Invest Ophthalmol Vis Sci*. 2021;62(8):2982.

Appendix

Here we articulate the derivation of, and the logic behind, the magnification calculations. Among these elaborations, some text and equations are repeated from the Methods for continuity of the derivation.

Definitions, Conventions, and Assumptions

We consider the fovea as the origin (0,0,0) of a coordinate space with dimensions in millimeters, and distances along the visual axis from the retina to the nodal point are negative in sign (Fig. 1B). For ease of interpretation, field angles (θ) in radians are plotted in degrees, and when an object is at fixation the angle is 0°. Magnification is modeled up to a field angle of 105°, which covers the maximum extent of a healthy monocular visual field.[35] In this coordinate space, a two-dimensional section of retina can be described[1,27] using the conic section equation:[36]

$$0 = y^2 - 2rz + (Q+1)z^2 \tag{A1}$$

where y and z are coordinates in a Cartesian sense (Fig. 1), r is the vertex radius of curvature (that is, radius of curvature of the retina at the fovea), and Q is the conic constant that defines oblate ($Q > 0$; blue in Fig. 1B), spherical ($Q = 0$; green), prolate ($0 > Q > -1$; red), parabolic ($Q = -1$), and hyperbolic ($Q < -1$) profiles. Note that defining retinal shape with an elliptical conic section in Equation A1 is the general case, within which the specific case of a circular or spherical retina is included. Literature[36] contains an alternate definition of the conic constant using the symbol P, where $P = Q + 1$.

For some of the methods that follow, it is useful to manipulate Equation A1 to be in the form of the classical sagitta equation:

$$z = \frac{Cy^2}{\left(1 + \sqrt{1 - (1+Q)C^2y^2}\right)} \tag{A2}$$

where C is the retinal vertex curvature and $C = 1/r$.

Following optical convention, light is considered to travel in a straight line from left to right. We can, therefore, describe the path of a ray emerging from the nodal point (N') at angle θ and traveling toward the retina (such as in Fig. 1B) using the familiar straight-line equation:

$$y = (slope)\,z + y_{int} \tag{A3}$$

where

$$slope = \tan(\theta) \tag{A4}$$

and θ is positive if measured counterclockwise from the visual axis to the ray. The y-intercept of the straight line is

$$y_{int} = (-1)\,(slope)\,\left(N' \text{ to retina}\right) \tag{A5}$$

Checking Anatomical Plausibility and Nodal Point Position

There are various methods of measuring retinal shape,[1,2,27–29] each of which visualizes a different angular extent of retina. The representation in Figure 1B is similar to MRI studies[1,2] where a section through the entire eye globe is described by a single ellipse. Although fitting smaller angular portions of the retina[27] might provide more accurate fitting over those segments, if the fit parameters are extrapolated to describe an entire eye globe it opens the possibility of anatomically implausible eye shapes. For example, if a posterior section of retina is best fit by a parabolic conic section, the anterior part of that hypothetical eye will never close at all, and axial length (Equations 2 and A6) in the magnification calculations is undefined. Alternatively—at the other extreme of asphericity—if a segment of posterior retina is described by a substantially oblate ellipse, it is possible that the extrapolated full ellipse will be too short to plausibly define an anatomically typically axial length. Therefore, if only a segment of the retina has been fit, it is prudent to determine whether an elliptical fit to that segment can be meaningfully extended to define an entire eye. To check this plausibility, we begin by calculating axial length from the parameters that define the eye shape:

$$Axial\ length = \frac{-2r}{(Q+1)} \tag{A6}$$

Recall, in our representation, r is measured from the vertex to the center of curvature and is a negative distance. For segments of posterior retinal profiles that are fit with parabolic ellipses ($Q = -1$) (and will not converge to form an anterior portion of an eye), the denominator of Equation A6 becomes zero and axial length is undefined.

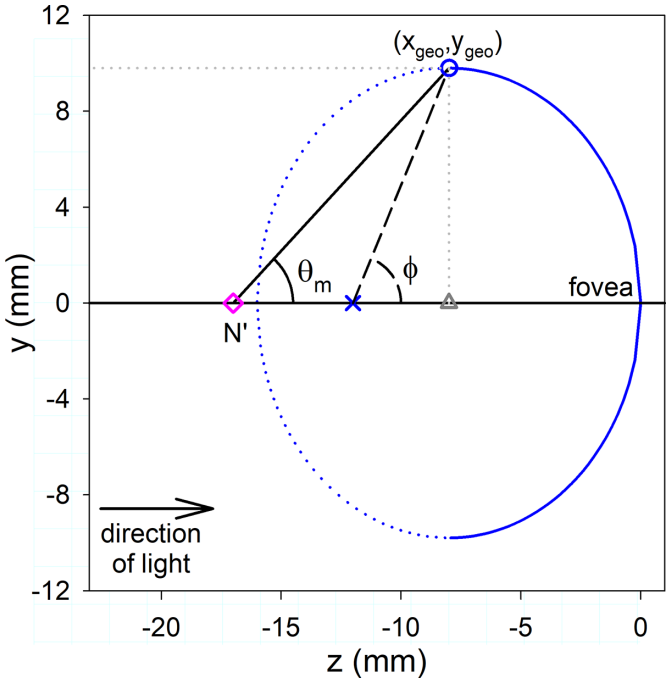

Figure A1. Limiting the field angles over which magnification is calculated when only a segment of the retina has been fit. Here, a retinal segment has been fit with an oblate ellipse ($r = -12$ mm, $Q = 0.5$, $N' = -17$ mm from the retina). If the fit parameters are extrapolated to define an entire eyeball, the modeled axial length is 16 mm, which is nearer to the retina than the nodal point. In this case, the extent of field angles over which magnification is calculated is limited to the angle (θ_m) where a ray from N' intersects at the maximum y-extent of the retina (x_{geo}, y_{geo}). The *gray triangle* is the geometric center of the fitted ellipse.

If the calculated axial length (Equation A6) is greater in magnitude than the distance from the nodal point (N') to the retina, then any ray will reach the retina irrespective of the angle at which it emerges from the nodal point, and the magnification calculations do not need to be restricted. However, if only a segment of retina has been fit with an oblate ellipse and those fit parameters are extrapolated to define an entire eyeball, it is possible that the nodal point may be farther from the fovea than the hypothetical axial length (Fig. A1). In such cases, we limit that calculation of magnification to the maximum y-value (immediately before the retina begins to curve back towards the visual axis). For any ellipse (or circle), the z-value at which that happens is the midpoint of the theoretical axial length, which corresponds to the z-value of the geometric center (z_{geo}) of the ellipse and half of the value determined by Equation A6 (illustrated in Fig. A1). Here, z_{geo} is a negative distance relative to the fovea. The maximum y-value (y_{geo}) can be calculated by substituting z_{geo} into Equation A1 and solving for y. Alternatively, a simpler calculation of y_{geo} is possible by noting that the point where the retinal shape begins curving back toward the visual axis is when the square root in the denominator of Equation A2 is not real; thus, when

$$(1 + Q)\, C^2 y^2 > 1 \tag{A7}$$

and the point immediately before the retina begins curving back (that is, the maximum y-value) is when

$$(1 + Q)\, C^2 y^2 = 1 \tag{A8}$$

Equation A8 can be easily manipulated such that

$$y_{geo} = \sqrt{\frac{1}{(1 + Q)\, C^2}} \tag{A9}$$

Then, in the case where the nodal point is farther from the fovea than the hypothetical axial length given by Equation A6, the maximum valid field angle where a ray from the posterior nodal point will intersect with the retinal asymptote is

$$\theta_m = \arctan\left(\frac{y_{geo}}{(z_{geo} - N')}\right) \tag{A10}$$

where y_{geo} is positive and z_{geo} and N' are negative.

Mapping an Angle at the Nodal Point to the Geometric Center of an Ellipse

Now that we understand the position of the nodal point relative to the theoretical axial length, as well as the maximum valid field angle, we can begin to calculate local retinal magnification in the radial meridian. First, we find the intersection point k (z_{int},y_{int}) on the retina of a ray emerging from the nodal point at angle θ. This is accomplished by formulating Equations A1 and A3 in terms of y, setting them equal to each other, and solving for the roots of z using the classical *quadratic formula*:

$$\sqrt{2rz - (Q + 1)\, z^2} = (slope)\, z + y_{int} \tag{A11}$$

which reduces to

$$0 = (-1 - Q - (slope^2))\, z^2 + (2r - 2\,(slope)\,(y_{int}))\, z - y_{int}^2 \tag{A12}$$

The roots of z from the general quadratic formula are

$$z_r = \frac{-B \pm \sqrt{B^2 - 4AC}}{2A} \tag{A13}$$

where, from Equation A12, A and B are the coefficients of z^2 and z, respectively, and C is the constant term;

that is,

$$A = \left(-1 - Q - \left(slope^2\right)\right)$$
$$B = \left(2r - 2\left(slope\right)\left(y_{int}\right)\right)$$
$$C = \ -y_{int}^2$$

The y-coordinates corresponding to each z-root are calculated by substituting each z_r (Equation A13) into either Equation A1 or Equation A3. Because θ is measured counterclockwise, we select the z-root that corresponds to a positive y-coordinate.

The angle subtended by the intersection point (z_{int}, y_{int}) at the nodal point is θ; in the next section, we will require the angle (ϕ) subtended by the same retinal point at the geometric center of the ellipse (Fig. 1B). The quadrant-specific arctangent formulation is

$$\Phi = ATAN2\left(\left(z_{int} - z_{geo}\right),\ \left(y_{int} - 0\right)\right) \qquad \text{(A14)}$$

where y_{int} is positive and z_{int} and z_{geo} are negative.

Calculation of Radial Local Retinal Magnification

The derivation of the radial magnification equations begins with the classical geometric definition of the perimeter (circumference) of an ellipse (Equation A15).[57] Calculation of tangential magnification will follow from the radial method.

$$Perimeter = 4a\int_0^{\pi/2}\sqrt{1 - e^2 sin^2\Phi}\,d\Phi \qquad \text{(A15)}$$

where a is the length of the semi-major axis of the ellipse, ϕ is the angle subtended at the geometric center of the ellipse (not at the nodal point; see Fig. 1B), and e is the ellipse eccentricity defined as

$$e = \sqrt{1 - \left(b^2/a^2\right)} \qquad \text{(A16)}$$

where b is the length of the semi-minor axis of the ellipse. For the spherical or circular case, $a = b$ and $e = 0$. For all retinal shapes, we have already calculated magnitudes of a and b under other names above:

$$a = \left|z_{geo}\right| = \left|\frac{r}{(-Q-1)}\right| \qquad \text{(A17)}$$

$$b = \left|y_{geo}\right| = \left|\sqrt{\frac{1}{(1+Q)\,C^2}}\right| \qquad \text{(A18)}$$

Note that ellipse eccentricity captures only the relative lengths (proportionality) of the major and minor semi-axes; hence, infinitely many mathematically *similar* ellipses can all have identical eccentricity. Also note that a is always for the major (longer) axis and b is always the minor (shorter) axis; therefore, ellipse eccentricity is insensitive to prolate or oblate orientations (conic constant Q).

Local magnification (mm/deg) at angle ϕ is the first derivative of the perimeter function (mm). Hence, differentiating Equation A15 gives

$$Magnification = 4a\sqrt{1 - e^2 sin^2\Phi} \qquad \text{(A19)}$$

Because, at this point, we desire only the relative pattern of radial magnification as function of field angle, and magnification will be scaled to the parameters of a particular eye and nodal point in the next step, the constant factors that scaled the integral are omitted:

$$Local\ relative\ magnification$$
$$= mag_{rel}\left(\Phi\right) = \sqrt{1 - e^2 sin^2\Phi} \qquad \text{(A20)}$$

From Equation A20 we have determined local magnification as a function of angle (ϕ) for a retina with elliptical eccentricity of e.

Finally, local radial magnification as function of field angle θ and specific to the dimensions of the given retina and the location of the nodal point is calculated as the product of three values described below: (1) local relative magnification, (2) the size of the angle subtended at the geometric center by an angle subtending 1° at the nodal point (N'), (3) and the magnification relative to the geometric center at the ellipse vertex (fovea). These methods are automated in a spreadsheet in the Supplementary Materials. First, local relative magnification is from Equation A20. Second, if an angle subtending 1° is projected from the nodal point and centered around the ray at the angle of interest θ, then the angle subtended at the geometric center is calculated using Equations A3, A4, A5, A12, A13, and A14. Third, when the field angle (θ) is zero, magnification is determined by the distance along the visual axis to the vertex. Here, that distance is from the geometric center and

$$mag\left(0^\circ\right) = \frac{\pi\left|z_{geo}\right|}{180} \qquad \text{(A21)}$$

where $\pi/180$ is the conversion of 1° to radians.

Calculation of Tangential Local Retinal Magnification

Calculations of tangential magnification assume the eye globe to be an ellipsoid of rotation about the axial z-axis (Fig. 1A). Tangential magnification is ultimately calculated using Equation A21 and substituting the path length of the ray (from the nodal point to the

retina) in the place of z_{geo}. Briefly, we articulate the logic leading to that conclusion.

By definition, tangential magnification is along a meridian orthogonal to the radial fit—that is, in the cyan plane in Figure 1C. The intersection of a plane and an ellipsoid is an ellipse (dotted red ellipse in Fig. 1A). That ellipse can be remapped from three dimensions into two dimensions (into the cyan plane), and the original intersection point of the ray and retina (k) can be defined as the new origin of this new two-dimensional space. Having an ellipse with the vertex at the new origin of this coordinate space, we can again apply the magnification method described above. Because instantaneous tangential magnification relates to the path length of ray from the nodal point to the retina, tangential magnification is determined by substituting that path length into Equation A21.

The geometry of the calculations was visualized and the magnification values verified using The Geometer's Sketchpad (McGraw-Hill). During other work by our group,[58] good agreement was found between Zemax, which defines and traces rays with reference to the entrance pupil, and the present method that uses the nodal point, echoing other widefield findings.[32]